PHYSICAL REVIEW E, VOLUME 65, 055101(R)

Drifting pattern domains in a reaction-diffusion system with nonlocal coupling

Ernesto M. Nicola, Michal Or-Guil, Wilfried Wolf, and Markus Bär
Max-Planck-Institut für Physik komplexer Systeme, Nöthnitzer Straße 38, D-01187 Dresden, Germany
(Received 19 May 2000; revised manuscript received 18 January 2002; published 24 April 2002)

Drifting pattern domains (DPDs), i.e., moving localized patches of traveling waves embedded in a stationary (Turing) pattern background and vice versa, are observed in simulations of a reaction-diffusion model with nonlocal coupling. Within this model, a region of bistability between Turing patterns and traveling waves arises from a codimension-2 Turing-wave bifurcation (TWB). DPDs are found within that region in a substantial distance from the TWB. We investigated the dynamics of single interfaces between Turing and wave patterns. It is found that DPDs exist due to a locking of the interface velocities, which is imposed by the absence of space-time defects near these interfaces.

DOI: 10.1103/PhysRevE.65.055101 PACS number(s): 82.40.Ck, 47.54.+r

INTRODUCTION

Pattern forming processes in nonequilibrium systems can be classified according to the primary instability of the spatially homogeneous state. Reference [1] distinguishes three basic types of instability in unbounded systems: (i) spatially periodic and stationary in time, (ii) spatially periodic and oscillatory in time, and (iii) spatially homogeneous and oscillatory in time. Within the reaction-diffusion literature, these instabilities are known as Turing, wave, and Hopf bifurcations, respectively.

Many chemical and biological patterns are well captured by so called activator-inhibitor models [2] describing the dynamics of two reacting and diffusing substances with two coupled partial differential equations. In such two-component reaction-diffusion models only Turing and Hopf instabilities are possible. Recently, numerical investigations of chemical reaction-diffusion systems with three components [3] and nonlocal coupling [4] have yielded the occurrence of wave instabilities and the corresponding patterns. A universal description of patterns near these instabilities is achieved within the framework of amplitude equations [1,5].

Here, we study a simple FitzHugh-Nagumo model with inhibitory nonlocal coupling that is obtained as a limiting case of a three-component reaction-diffusion system. It describes the interaction of an activator species with an inhibitor. For slow inhibitor diffusion (compared to the activator diffusion), the model exhibits a wave instability, while for fast inhibitor diffusion, a Turing instability is found. The two instabilities occur simultaneously at a codimension-2 Turing-wave bifurcation (TWB). Such a situation has been found earlier within models for binary convection [6] and phase separation in reactive mixtures [7] and is a generalization of the well investigated Turing-Hopf instability in reaction-diffusion systems [8]. The basic properties of a TWB have been studied theoretically in amplitude equations [9] as well as experimentally in a one-dimensional gas-discharge system [10]. In our model, we find a pattern previously unknown in reaction-diffusion systems: drifting pattern domains (DPDs), i.e., localized patches of traveling waves embedded in a Turing background and vice versa (see Fig. 1). These patches have constant width and move (drift) with constant speed. They exist in a broad region of the parameter space embedded in a region of bistability between traveling waves and Turing patterns. Similar patterns have been reported in a variety of hydrodynamical experimental systems (see, e.g., [11,12]) and have been related to secondary instabilities (parity breaking) of stationary patterns [11,13].

In this Rapid Communication we show that it is sufficient to investigate the dynamics of single interfaces separating domains of Turing and wave patterns in order to understand the formation of DPDs. The dynamics of such interfaces is studied in the framework of amplitude equations and compared to results of numerical simulations in the original model. The dynamics of interfaces separating small amplitude patterns is well described by the amplitude equations. For large amplitude patterns, an effect arises that we call *velocity locking*. This locking mechanism is responsible for the existence of DPDs with constant width.

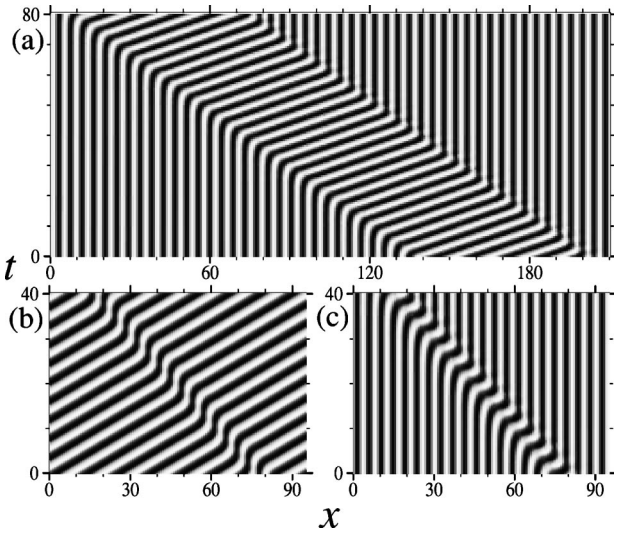

FIG. 1. Space-time plots of the field u in gray scale for three examples of DPDs found in numerical simulations of Eqs. (1). In all three cases $a=6.0$, and only a part of the system of length $L=409.6$ is shown. (a) Large DPD with $\delta=0.84$. (b),(c) DPDs consisting of a single cell of Turing and wave, respectively. In (b) $\delta=0.80$ and in (c) $\delta=0.91$. For other parameters, see [17].

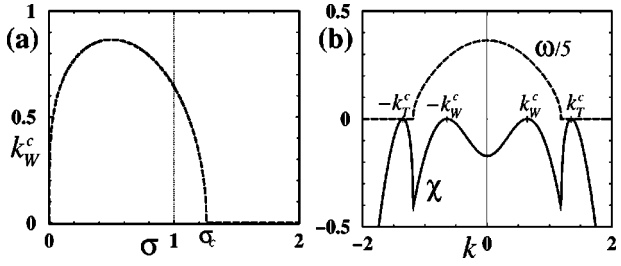

FIG. 2. (a) Critical wave number k_W^c against inverse nonlocal coupling range σ. (b) Real (χ) and imaginary part (ω) of $\lambda(k)$ at the TWB. For parameters, see [17].

MODEL EQUATIONS AND LINEAR STABILITY

We start from the three-variable system

$$\partial_t u = au + \beta u^2 - \alpha u^3 - bv - gw + \partial_x^2 u,$$

$$\partial_t v = cu - dv + \delta \partial_x^2 v,$$

$$\tau_w \partial_t w = eu - fw + \gamma \partial_x^2 w.$$

These equations are an extension of the FitzHugh-Nagumo model by a second inhibitor w. If the second inhibitor is very fast, $\tau_w = 0$, one finds

$$\partial_t u = au + \beta u^2 - \alpha u^3 - bv + \partial_x^2 u - \mu \int_{-\infty}^{+\infty} e^{-\sigma|x-x'|} u(x',t)\,dx',$$

$$\partial_t v = cu - dv + \delta \partial_x^2 v. \qquad (1)$$

The parameters characterizing the inhibitory nonlocal coupling in Eqs. (1) are then found as $\sigma = \sqrt{f/\gamma}$ and $\mu = g\sqrt{e^2/\gamma f}$ from the original three-variable model above. Related three-variable models have been introduced previously to describe pattern formation on seashells and in cell biology [14] as well as spot dynamics in gas discharges [15] and concentration patterns in heterogeneous catalysis [16]. Here, the emphasis is on the onset of pattern formation resulting from destabilization of a single homogeneous steady state.

Equations (1) possess the trivial homogeneous fixed point $\mathbf{u}_0 \overset{\text{def}}{=} (u_0, v_0)^T = (0,0)^T$ for all parameter values. Here, we consider the regime where this fixed point is the only one present and consider perturbations proportional to $e^{ikx - \lambda(k)t}$, where $\lambda(k) = \chi(k) + i\omega(k)$. The growth rates $\chi(k)$ are given by the eigenvalues of the Jacobian. Linear stability analysis reveals that Eqs. (1) exhibit wave instabilities if the nonlocal coupling is of sufficiently long range.

In the following we vary the control parameters a and δ; the "driving force" a represents the kinetics, whereas the ratio of diffusion coefficients δ describes the spatial coupling in the medium. All other parameters of Eqs. (1) have been fixed [17]. For the wave bifurcation, the critical wave number k_W^c and parameters a_W and δ_W are obtained from the condition $\lambda(k_W^c) = \pm i\omega_0$ where the perturbation with k_W^c is the fastest growing mode with $(k_W^c)^2 = \sqrt{2\mu\sigma/(1+\delta)} - \sigma^2$. Note that for both $\sigma \geqslant \sigma_C$ and $\sigma = 0$ (global coupling limit) the critical wave number is $k_W^c = 0$ [see Fig. 2(a)]. Similarly, a competing Turing instability appears for a critical parameter a_T with a wave number k_T^c, where the leading eigenvalue is $\lambda(k_T^c) = 0$. For large enough driving a, the wave instability appears for small δ, while for large δ the Turing instability destabilizes the homogeneous state. For the chosen parameter values, the system exhibits a TWB point [see Fig. 3(a) and [17]]. For the corresponding $\lambda(k)$, see Fig. 2(b).

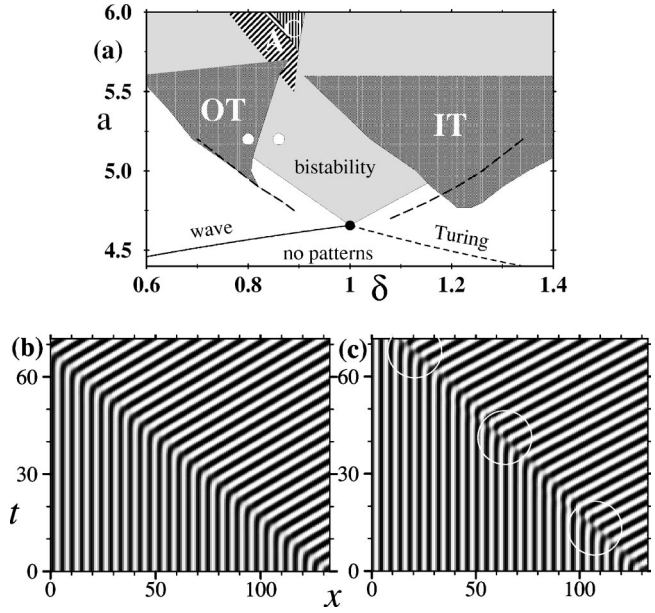

FIG. 3. (a) Parameter space a-δ near the TWB point (black circle). The light gray region indicates bistability between the Turing and wave pattern with k_T^c, k_W^c as predicted from Eqs. (2). Dark gray regions correspond to two examples of locking tongues for an outward interface with $k_T = k_T^c$ (region OT) and an inward interface with $k_W = k_W^c$ (region IT). These two tongues are shown only up to $a \approx 5.6$. The dashed lines show where the selected velocities of interfaces in Eqs. (2) coincide with v_{lock}. White circles indicate parameter values of simulations shown in (b) and (c). See Fig. 4 below for a description of the dashed regions. (b) and (c) show space-time plots of u in gray scale from simulations of Eqs. (1) showing outward interfaces for $a = 5.2$. In (b) an example inside the locking tongue is shown for $\delta = 0.80$ and in (c) an interface outside the tongue exhibiting defects (inside the white circles) for $\delta = 0.86$ is shown.

WEAKLY NONLINEAR ANALYSIS

Near the TWB, we can write $\mathbf{u} \overset{\text{def}}{=} (u,v)^T$ as a perturbative expansion around $\mathbf{u}_0$ using a small parameter ε, indicating the distance to the instability threshold: $\mathbf{u} = \mathbf{u}_0 + \varepsilon \mathbf{u}_1 + \varepsilon^2 \mathbf{u}_2 + \varepsilon^3 \mathbf{u}_3 + \cdots$, and use the following multiple scale ansatz:

$$\mathbf{u}_1 = [A(X,T_1,T_2)\mathbf{U}_A e^{i(\omega_0 t + k_W^c x)} + B(X,T_1,T_2)\mathbf{U}_B e^{i(\omega_0 t - k_W^c x)} + \mathcal{R}(X,T_1,T_2)\mathbf{U}_{\mathcal{R}} e^{ik_T^c x} + \text{c.c.}]/2.$$

This leads to a set of coupled equations for the amplitudes A, B, and $\mathcal{R}$ for left- and right-going waves and the Turing pattern that depend on slow time and space variables. The technical details of the derivation will be presented in a future publication [18]. The resulting equations read

$$\partial_t \mathcal{R} = \eta \mathcal{R} - |\mathcal{R}|^2 \mathcal{R} + \xi \partial_x^2 \mathcal{R} - \zeta(|A|^2 + |B|^2)\mathcal{R},$$

$$\partial_t A + c_g \partial_x A = \rho A + (1 + ic_1)\partial_x^2 A - (1 - ic_3)|A|^2 A - g(1 - ic_2)|B|^2 A - \nu(1 - i\kappa)|\mathcal{R}|^2 A,$$

$$\partial_t B - c_g \partial_x B = \rho B + (1 + ic_1)\partial_x^2 B - (1 - ic_3)|B|^2 B - g(1 - ic_2)|A|^2 B - \nu(1 - i\kappa)|\mathcal{R}|^2 B. \quad (2)$$

For the detailed values of all coefficients, see [19]. Note that the nonlocal term of Eqs. (1) enters into the diffusion coefficients of Eqs. (2) but does not give rise to nonlocal terms in Eqs. (2). Knowledge of the coefficients of Eqs. (2) allows analytical predictions of the pattern dynamics. Here, traveling waves are always preferred over standing waves ($g>1$, see [1]) and bistability between wave and Turing patterns is found ($\nu\zeta>1$). In this bistability region in parameter space [see Fig. 3(a)], a family of stable Turing patterns and two families of stable left- and right-traveling waves parametrized by their corresponding wave numbers coexist. To get further insight, we take a closer look at the dynamics of single interfaces separating domains of Turing and wave patterns.

SINGLE INTERFACE DYNAMICS

With suitable initial conditions, a moving interface between Turing and wave patterns will be formed in simulations of Eqs. (1). Near the interface that joins both patterns together, the maxima of the concentrations of activator u and inhibitor v are typically not conserved. As a consequence, space-time *defects* are produced by coalescence of maxima and minima [see Fig 3(c)].

There are two types of interface depending on whether the phase velocity of the waves points toward the interface or away from it. This classification is independent of the direction in which the interface is moving. In the following, we will call the first type *inward interfaces* and the second *outward interfaces*. Figures 3(b) and 3(c) show examples of the latter type.

Near the TWB, we have studied general properties of such interfaces in the amplitude equations (2) within a set of ordinary differential equations obtained from a coherent structure ansatz in the comoving frame [5]. Since the interface typically moves, we can distinguish an invading and an invaded domain. The wave numbers of Turing or wave patterns are not unique, since there exist sidebands of wavelengths around the respective critical wave numbers. Nevertheless, an interface will typically select a particular wave number for the invading domain, while the initial wave number of the invaded state is a free parameter [18]. The velocity of the interface is a function of this parameter. For invading Turing patterns the selected wave number is always the critical one, i.e., $k_T^{sel} = k_T^c$, while for invading waves typically $k_W^{sel} \neq k_W^c$ and therefore $\omega^{sel} \neq \omega_0$. This is valid for both inward and outward interfaces. Thus, we typically have two one-parameter families of interfaces for a given point in parameter space. Near the TWB, these results coincide quantitatively with numerical simulations of the nonlocal model (1).

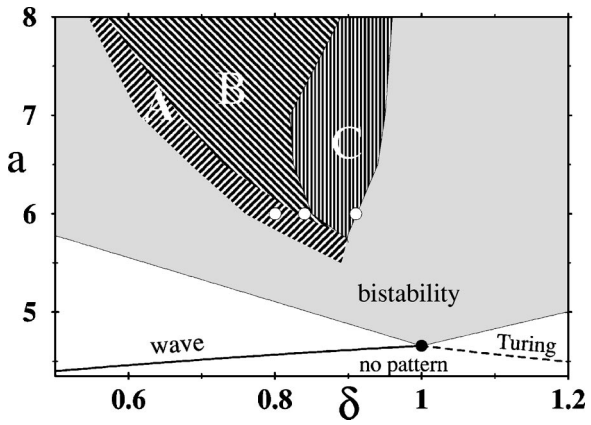

FIG. 4. The region of existence of DPDs obtained in simulations of Eq. (1) in the a-δ parameter space is shown dashed. The light gray area corresponds to the bistable region between the critical wave and Turing patterns as calculated from the amplitude equations (3). In region B DPDs of any size exist; the size being determined only by the initial condition. In region C small domains of wave patches traveling in a Turing background are found. In region A only Turing droplets are stable. The three circles correspond to the locations of simulations shown in Fig. 1.

Far away from the TWB, simulations of interfaces in Eqs. (1) show qualitatively similar behavior with respect to the selected wave numbers. In addition, interfaces far away from the TWB may exhibit a locking mechanism, where the selected velocity is determined by the absence of defects at the interface. For geometrical reasons an interface without defects, which connects a wave state with wave number k_W and frequency ω and a Turing state with k_T, has a speed $|v_{lock}| = \omega/(k_T - k_W)$. This velocity locking mechanism is found for both types of interface. The dark gray areas OT and IT in Fig. 3(a) show the regions in parameter space where velocity locking occurs (*locking tongues*) in the original reaction-diffusion equations (1) for outward and inward interfaces, respectively.

In contrast, there are no locking tongues in the corresponding amplitude equations (2) because the rapidly varying space and time scales have been factored out. However, on a line in the parameter space [see dashed line in Fig. 3(a)], the velocity of interfaces in Eqs. (2) coincides with the velocity prescribed by the locking mechanism. An example of a locked outward interface in Eqs. (1) is displayed in Fig. 3(b). Outside the corresponding tongue the outward interfaces display phase slips [see Fig. 3(c)]. The location of the locking tongues depends only weakly on the interface free parameter (k_W for inward and k_T for outward interfaces). Note that the locking tongues open at a substantial distance from the TWB. The locking mechanism arises when the characteristic

width of the interfaces is of the same order as the characteristic length scale of the patterns.

DPDs AND THEIR PHASE DIAGRAM

The locking mechanism found for single interfaces allows us to understand the existence of DPDs. Indeed, as can be seen in Fig. 1, DPDs do not show defects. Large DPDs are composed of an inward and an outward interface [see Fig. 1(a)], which are both subject to interface locking. This implies that the velocities of both interfaces have equal magnitude $|v_{lock}|$ but opposite signs. Therefore, the DPDs maintain *constant* but *arbitrary* width. Furthermore, the region of parameter space where large DPDs exist starts to open where the locking tongues for both interface types begin to overlap [see Fig. 3(a)]. This is the case for $a \gtrsim 5.7$. Above that value, DPDs spontaneously form from a variety of initial conditions. We have determined the parameter region where they propagate with constant width and drift speed, from extensive simulations in systems with sizes $L > 400$ and periodic boundary conditions. The results are shown in the phase diagram of Fig. 4.

We can distinguish three different subregions. In region *B*, DPDs of any size, with two locked interfaces traveling at the same speed, are found [see Fig. 1(a)]. In region *A*, the inward interface is no longer locked and its speed is smaller than $|v_{lock}|$. Therefore, large domains of Turing (wave) patterns contract (expand) in size until only a stable DPD containing a single Turing cell is left [see Fig. 1(b)]. In region *C*, the outward interface selects a k_W^{sel} that would be unstable against Turing patterns in an infinite domain. Therefore, the wave domain forming the DPD is mostly replaced by a Turing pattern. However, small DPDs with a few wavelengths of wave pattern are still encountered. At the outer boundary of region *C*, only DPDs with a single wave cell are found to be stable [see Fig. 1(c)].

CONCLUSION

We found drifting pattern domains in a reaction-diffusion model with nonlocal coupling. Their ingredients include a bistability between wave and Turing patterns near a codimension-2 point as well as absence of defects at the interface. They exist as robust patterns only in a finite distance to the onset of pattern formation as a consequence of velocity locking of the constituting interfaces. We expect that such a locking mechanism is not limited to the reaction-diffusion model studied here and should carry over to other physical systems with competing patterns. Altogether, DPDs and their constituting interfaces represent a generalization of simpler structures such as fronts and pulses in bistable reaction-diffusion systems, which do not simply combine two homogeneous states, but, instead, select their constituents from whole families of possible traveling or stationary periodic patterns.

[1] M.C. Cross and P.C. Hohenberg, Rev. Mod. Phys. **65**, 851 (1993).

[2] A.S. Mikhailov, *Foundations of Synergetics I* (Springer-Verlag, New York, 1990).

[3] A.M. Zhabotinsky, M. Dolnik, and I.R. Epstein, J. Chem. Phys. **103**, 10 306 (1995).

[4] M. Hildebrand, A.S. Mikhailov, and G. Ertl, Phys. Rev. Lett. **81**, 2602 (1998).

[5] M. van Hecke, C. Storm, and W. van Saarloos, Physica D **134**, 1 (1999).

[6] W. Schöpf and W. Zimmermann, Phys. Rev. E **47**, 1739 (1993).

[7] T. Okuzono and T. Ohta, Phys. Rev. E **64**, 045201 (2001).

[8] J.J. Perraud *et al.*, Phys. Rev. Lett. **71**, 1272 (1993); A. De Wit *et al.*, Phys. Rev. E **54**, 261 (1996); M. Meixner *et al.*, *ibid.* **55**, 6690 (1997); M. Or-Guil and M. Bode, Physica A **249**, 174 (1998).

[9] D. Walgraef, Phys. Rev. E **55**, 6887 (1997).

[10] H. Willebrand *et al.*, Contrib. Plasma Phys. **31**, 57 (1991).

[11] J.M. Flesselles, A.J. Simon, and A.J. Libchaber, Adv. Phys. **1**, 1 (1991).

[12] C. Counillon *et al.*, Phys. Rev. Lett. **80**, 2117 (1998); M. Ginibre, S. Akamatsu, and G. Faivre, Phys. Rev. E **56**, 780 (1997).

[13] R.E. Goldstein *et al.*, Phys. Rev. A **43**, 6700 (1991).

[14] H. Meinhardt and M. Klingler, J. Theor. Biol. **126**, 63 (1987); H. Meinhardt, J. Cell. Sci. **112**, 2867 (1999).

[15] C.P. Schenk *et al.*, Phys. Rev. Lett. **78**, 3781 (1997); M. Or-Guil *et al.*, Phys. Rev. E **57**, 6432 (1998).

[16] M. Sheintuch and O. Nekhamkina, J. Chem. Phys. **107**, 8165 (1997).

[17] We chose the parameters $b=4$, $c=d=1$, $\sigma=1$, $\mu=2$, $\alpha=4/3$, and $\beta=0$. All results have been checked for $\beta \neq 0$ and do not change qualitatively as long as $|\beta|$ is not too large. The TWB point is found at $a_{TW}=4\sqrt{2}-1$ and $\delta_{TW}=1$ with $k_T^c=\sqrt{2^{3/2}-1} \simeq 1.352$, $k_W^c=\sqrt{2^{1/2}-1} \simeq 0.644$, and $\omega_0=\sqrt{2}$.

[18] E. Nicola, M. Or-Guil, and M. Bär (unpublished).

[19] At the TWB point for the parameters given in [17] the coefficients of Eqs. (2) are $c_g=1.1892$, $c_1=0.8536$, $c_3=1$, $g=2$, $c_2=1$, $\nu=1/2$, $\zeta=8$, $\kappa=1$, and $\xi=4.4142$. The small parameters in Eqs. (2) are defined by $\rho=[(a-a_{TW})-(k_W^c)^2(\delta-\delta_{TW})]/2$ and $\eta=2[(a-a_{TW})+(k_T^c)^2(\delta-\delta_{TW})/2]$.